Propagation of a hole on a Néel background

E. Müller-Hartmann and C. I. Ventura*
Institut für Theoretische Physik, Universität zu Köln, Zülpicher Straße 77, Köln 50937, Germany
(Received 28 February 1994)

We analyze the motion of a single hole on a Néel background, neglecting spin fluctuations. Brinkman and Rice studied this problem on a cubic lattice, introducing the retraceable-path approximation for the hole Green's function, exact in a one-dimensional lattice. Metzner *et al.* showed that the approximation also becomes exact in the infinite-dimensional limit. We tackle this problem by resumming the Nagaoka expansion of the propagator in terms of nonretraceable skeleton paths dressed by retraceable-path insertions. This resummation opens the way to an almost quantitative solution of the problem in all dimensions and, in particular, sheds light on the question of the position of the band edges. We studied the motion of the hole on a double chain and a square lattice, for which deviations from the retraceable-path approximation are expected to be most pronounced. The density of states is mostly adequately accounted for by the retraceable-path approximation. Our band-edge determination points towards an absence of band tails extending to the Nagaoka energy in the spectra of the double chain and the square lattice. We also evaluated the spectral density and the self-energy, exhibiting k dependence due to finite dimensionality. We find good agreement with recent numerical results obtained by Sorella *et al.* with the Lanczos spectra decoding method. The method we employ enables us to identify the hole paths which are responsible for the various features present in the density of states and the spectral density.

I. INTRODUCTION

The discovery of high-temperature superconductivity has intensified the interest in the study of strongly correlated electron systems. Among the important related subjects awaiting solution is the dynamics of holes in the presence of a spin background. Among pioneering works on the problem one can cite that by Bulaevskii, Nagaev, and Khomskii[1] who, studying the motion of a hole on an antiferromagnetic background, with the neglect of quantum fluctuations, introduced the "string potential" concept. As the hole moves on the Néel background it leaves behind a string of overturned spins, thus increasing the exchange energy proportionally to the length of the string. This can lead to self-trapped (or, as they were called in Ref. 1, "quasioscillator") states centered at the original position of the hole. Two years later, Brinkman and Rice[2] studied the motion of a single hole on different spin backgrounds, employing the Nagaoka expansion for the hole propagator.[3] This involves contributions by hole paths restoring the spin background, classified according to their length. For a cubic lattice and ferromagnetic, antiferromagnetic, and random spin backgrounds, they calculated the exact contributions of hole paths up to length 10, neglecting spin fluctuations. The density of states obtained was compared with the one resulting from considering only the self-retracing paths of the hole, the "retraceable-path approximation"(denoted RPA throughout this paper). In this approximation, which does not distinguish between different spin backgrounds, one can exactly sum the series for the propagator, which involves only local contributions, thus obtaining no momentum (k) dependence: The motion is completely incoherent. With the RPA Brinkman and Rice[2] were able to account for the body of the band in the case of a Néel background. Less agreement was obtained[2] for the random background, while the ferromagnetic case reduces to the uncorrelated single-particle motion in a tight-binding band which generally is quite different from the RPA description. They also observed that the RPA became exact in the one-dimensional case where, for any spin background, the free-particle result is obtained. The band edges appear at the so-called Nagaoka energies.

In a series of recent works[4,5] the motion of a hole on a spin background was analyzed in the case of infinite dimensions. In particular, Metzner *et al.*[4] estimated the contributions to the propagator in terms of the dimension (D). Neglecting spin fluctuations, the only nonretraceable contributions which would remain finite at $D = \infty$ would be those of loop paths circulated only once. These would certainly not preserve a Néel-ordered spin background, so that the RPA becomes the exact solution of the problem in this case. For the Néel background at finite dimensions, the lowest-order corrections to the RPA density of states in the case of a hypercubic lattice would come from circulating elementary square plaquettes three times (thus of order $\sim 1/D^4$). More important are the nonlocal corrections to the propagator, the lowest of which is of order $\sim 1/D$ (the hole can propagate to nearest neighbor sites on the same sublattice circulating an elementary square plaquette one and a half times). The latter corrections would give rise to a k-dependent self-energy for the hole. Trugman[6] already mentioned these nonretraceable paths in his study of the two-dimensional Hubbard antiferromagnet. Quite different physics is expected when the quantum fluctuations associated with transverse exchange interactions

are taken into account from the start. This problem has been addressed in many recent works; among others see Refs. 7–13.

Taking into account the results mentioned above for hole motion on a Néel background in the absence of quantum fluctuations, we propose here a method to evaluate the local and nonlocal parts of the propagator in order to analyze the departures from the RPA for reduced dimensionality. In Sec. II we describe the method employed to obtain these quantities. Basically, the Nagaoka expansion of the propagator is rewritten in terms of nonretraceable skeleton paths dressed by retraceable paths. Though one can explicitly evaluate the contribution of a dressed skeleton diagram of given length, one has to determine numerically the numbers of bare background-restoring skeleton paths. The results obtained with this method for the double chain and the square lattice are presented in Sec. III. We can quite reliably determine the band edges, and our results place them at an intermediate value between the RPA edge and the Nagaoka energy. In general, we find good agreement with the recent numerical results of Zhong *et al.*,[14] obtained with the Lanczos spectra decoding method. The method we employ enables us to determine the origin of the distinctive features exhibited by the density of states and the spectral density. Thus, we can identify the relevant paths responsible for the k dependence at reduced dimensionality. In Sec. IV we summarize our results.

II. ANALYTICAL METHOD

In this section we describe the method employed to evaluate the hole propagator on a Néel background, in which spin fluctuations are neglected.

The Nagaoka expansion[3,4] for the Green's function G describing the propagation of a hole inserted into an arbitrary fixed spin configuration $|\, s\rangle$ takes the following form:

$$\begin{aligned} G^s_{i,j}(w) &= \sum_\sigma \left\langle s \left| c^\dagger_{i,\sigma} \frac{1}{w-H} c_{j,\sigma} \right| s \right\rangle \\ &= \frac{1}{w}\left[\delta_{i,j} + \sum_{n=1}^{\infty} A^s_{i,j,n}\left(\frac{-t}{w}\right)^n\right], \\ H &= -t \sum_{\langle i,j\rangle,\sigma} [\,(1-n_{i,-\sigma}) c^\dagger_{i,\sigma} c_{j,\sigma} (1-n_{j,-\sigma}) \\ &\quad + \text{H.c.}\,]. \end{aligned} \tag{1}$$

Above, $c^\dagger_{i,\sigma}$ ($c_{i,\sigma}$) creates (annihilates) a particle with spin σ at the lattice site i, while H is the Hamiltonian describing the correlated hopping of a particle between nearest neighbor sites. The coefficients $A^s_{i,j,n}$ denote the number of distinct n-step paths of the hole in the spin background s which start at site j and end at site i, restoring the original spin configuration after the last step. In particular we will consider the case of a Néel spin background, $s = N$, where propagation is only possible between sites belonging to the same sublattice.

As we mentioned in the previous section, the paths in which the hole completely retraces its steps are the only relevant ones at $D = \infty$ on a Néel background.[4] Even at finite dimensions they would determine the leading terms of the local Green's function. Following Brinkman and Rice[2] one can derive the RPA propagator by introducing the following irreducible "self-energy" S (here irreducibility means that the path cannot be split up into two or more consecutive retraceable paths):

$$G_{\text{RPA}}(w) = \frac{1}{w[1-S(w)]}. \tag{2}$$

The lowest-order RPA self-energy will derive from the contributions of single jumps to a nearest neighbor and immediate return to the origin, so that

$$S^0(w) = Z\left(\frac{t}{w}\right)^2, \tag{3}$$

where Z is the number of nearest neighbors. The next-order irreducible self-energy contribution consists of one jump to a nearest neighbor of the origin followed by a further jump in any direction different from the previous jump [thus having $(Z-1)$ possibilities for this step] before retracing the whole path. In general, one can write the RPA irreducible self-energy as

$$S(w) = Z\left(\frac{t}{w}\right)^2 C(w), \tag{4}$$

$$\begin{aligned} C(w) &= 1 + \left(\frac{Z-1}{Z}\right) S(w) + \left(\frac{Z-1}{Z}\right)^2 S(w)^2 + \cdots \\ &= \frac{1}{1-\left(\frac{Z-1}{Z}\right) S(w)}; \end{aligned} \tag{5}$$

that is, it is written self-consistently in terms of the jump to a nearest neighbor of the origin dressed by retraceable paths, where C is the RPA-dressed irreducible vertex part.

The solution of the self-consistent system of equations (4) and (5) is[2]

$$S(w) = \frac{Z}{2(Z-1)}\left[1 - \sqrt{1-4(Z-1)\left(\frac{t}{w}\right)^2}\right]. \tag{6}$$

Therefore the RPA propagator is given by

$$G_{\text{RPA}}(w) = \frac{1}{w - \frac{Z}{2(Z-1)}\left[w - \sqrt{w^2 - 4(Z-1)t^2}\right]}. \tag{7}$$

From this expression one can easily determine the band edges, $\pm w_{\text{RPA}}$, of the energy spectrum obtained in the RPA for a hole hopping on a Néel background as

$$w_{\text{RPA}} = 2\sqrt{Z-1}\,t, \tag{8}$$

which exhibits a reduction from the free-particle value (Nagaoka energy), $w_{\text{FP}} = Zt$ for $Z > 2$, while the RPA coincides with the free-particle result in the one-dimensional ($Z = 2$) case, as already mentioned in the previous section.

Having introduced the retraceable-path approximation (RPA) which gives a good approach to the local propa-

gator, we will now describe the method we employed to obtain the Green's function of a hole moving on a Néel background. In the Nagaoka expansion (1) we take into account all background-restoring paths in the following way: For each path length, we take all possible nonretraceable "skeleton" paths which restore the Néel background, and dress them by inserting all possible retraceable paths. The RPA paths result from dressing the trivial skeleton path of length 0. For all other skeleton paths two types of dressing have to be taken into account: (1) additional steps within the skeleton path (internal dressing), (2) irreducible RPA vertex parts inserted at all vertices of the internally dressed skeleton path. To avoid double counting one has to distinguish between external and internal vertices in the internally dressed skeleton diagram. External vertices are connected by one link to the skeleton which implies only one forbidden first step for all retraceable-path insertions. The dressed "external" vertex $C_{\mathrm{ex}}(w)$ is therefore correctly described by Eq. (5). Internal vertices, however, are doubly connected to the skeleton path, such that two first steps are forbidden for insertions of the retraceable-path vertex dressings. Therefore, the RPA-dressed irreducible internal vertex part is

$$C_{\mathrm{in}}(w) = \frac{1}{1-\left(\frac{Z-2}{Z}\right)S(w)}. \tag{9}$$

In order to perform the dressing we have to count the number of internal dressings which can be considered for a skeleton diagram of length l. For this we define $N_l^k(m,n)$ as the number of paths of m steps on a skeleton diagram of length l, starting at site 0, reaching site $k\,(0 \le k \le l)$ after step m, and visiting the end points 0 and l exactly n times (including the start at site 0). In terms of these numbers the dressed contribution of a single skeleton diagram of length l to the propagator is given by

$$G_l(w) = \frac{1}{w}\left[\sum_{m,n} N_l^l(m,n)\left(\frac{t}{w}\right)^m C_{\mathrm{in}}^{m+1-n} C_{\mathrm{ex}}^n\right]. \tag{10}$$

For the numbers $N_l^k(m,n)$ the following recursive system of equations holds:

$$\begin{aligned} N_l^0(0,n) &= \delta_{n,1}, \\ N_l^0(m+1,n+1) &= N_l^1(m,n), \\ N_l^k(m+1,n) &= N_l^{k+1}(m,n) + N_l^{k-1}(m,n) \qquad (0<k<l), \\ N_l^l(m+1,n+1) &= N_l^{l-1}(m,n). \end{aligned} \tag{11}$$

One can solve these equations by introducing the generating functions

$$g_k(x,y) = \sum_{m,n} N_l^k(m,n) x^m y^n, \tag{12}$$

and rewriting Eqs. (11) in terms of them. One obtains

$$g_0(x,y) = y + xy g_1(x,y), \tag{13}$$

$$g_k(x,y) = x\left[g_{k-1}(x,y) + g_{k+1}(x,y)\right] \qquad (0<k<l), \tag{14}$$

$$g_l(x,y) = xy g_{l-1}(x,y). \tag{15}$$

The general solution of Eq. (14) is given by

$$g_k(x,y) = a_+(x,y)\eta_+^k(x) + a_-(x,y)\eta_-^k(x), \tag{16}$$

with

$$\eta_\pm(x) = \frac{1}{2x}\left(1 \pm \sqrt{1-4x^2}\right) \equiv \eta_\pm. \tag{17}$$

The coefficients $a_\pm$ are finally determined from the equations for g_0 and g_l, (13) and (15), and one obtains

$$g_l(x,y) = \frac{xy^2\,(\eta_+ - \eta_-)}{\eta_+^l\,(1-xy\eta_-)^2 - \eta_-^l\,(1-xy\eta_+)^2}. \tag{18}$$

This generating function can be viewed as the Green's function of a particle propagating on a linear chain of length l with hopping amplitudes at the edge bonds different from the internal ones.[15]

From Eqs. (10) and (12) we see that the contribution of a dressed skeleton diagram of length l is determined as

$$G_l(w) = \frac{C_{\mathrm{in}}(w)}{w}\, g_l\left(\frac{tC_{\mathrm{in}}(w)}{w}, \frac{C_{\mathrm{ex}}(w)}{C_{\mathrm{in}}(w)}\right). \tag{19}$$

For the special values of the variables of $g_l(x,y)$ appearing in Eq. (19) the expression (18) simplifies considerably since $1 - xy\eta_+(x) \equiv 0$. We therefore obtain the very simple final result

$$G_l(w) = G_{\mathrm{RPA}}(w)\left(\frac{2t}{w+\sqrt{w^2-w_{\mathrm{RPA}}^2}}\right)^l, \tag{20}$$

which holds even for $l = 0$, although our derivation did not include this case.

In terms of these dressed skeleton diagram contributions we can now write the propagator as

$$G_{i,j}^N(w) = \sum_{l=0}^{\infty} K_{i,j}^l G_l(w), \tag{21}$$

where $K_{i,j}^l$ is the number of different bare background-restoring skeleton paths of l steps between the end points i and j. On a Néel background only skeleton paths composed of an even number of steps l will contribute, as sites i and j must belong to the same sublattice. Trivially, considering that $K_{i,j}^0 = \delta_{i,j}$, the RPA is contained in the propagator of Eq. (21).

Equation (21) represents a resummation of the Nagaoka expansion (1) motivated by the merits of the RPA. As we will show in the next section, it can be used quite efficiently because the number of skeleton paths of length l is much smaller than the total number of paths of the same length. As discussed in the Introduction, the contributions from nonretraceable paths get less important the higher the dimension of the lattice. Therefore, we have chosen the two nontrivial systems of lowest dimension to demonstrate the usefulness of Eq. (21): the double chain

and the square lattice.

The resummation (21) opens a new chance for a qualified discussion of the band-edge problem. Brinkman and Rice[2] have given an argument which would suggest that the spectrum of the correlated hole motion on a Néel background extends to the Nagaoka energy $w_{\rm FP} = Zt$, via exponential band tails. Zhong *et al.*[14] appear to provide evidence in favor of this scenario by showing that their spectrum extrapolates to the Nagaoka energy. In our opinion, both the Brinkman-Rice argument and the evidence of Zhong *et al.* are not conclusive. It is, in fact, obvious from a total spin decomposition of the Néel state that the spectrum extends to $w_{\rm FP}$ for finite size systems: The maximum spin $S = L/2$ is contained in an L-site Néel background with a probability of order 2^{-L}. Therefore the issue is not at all whether the spectrum extends to $w_{\rm FP}$ for systems of sufficient size, as demonstrated by the extrapolation in Ref. 14, but rather whether this part of the spectrum survives with a finite weight in the thermodynamic limit. The results we present in the next section point to band edges below $w_{\rm FP}$.

The position of the band edge is related to the radius of convergence of the series in Eq. (21). If we replace the series by any finite summation, the band edge remains at the RPA value (8). An extension of the spectrum beyond this value can only result from the series diverging for energies $w \leq w_c$ with $w_c > w_{\rm RPA}$. One can quite generally assume an exponential increase in the number of skeletons with the path length:

$$K^l_{i,j} \propto \alpha^l \qquad (l \to \infty). \tag{22}$$

This determines the radius of convergence, which using Eq. (20) gives the following simple relation between the position of the band edge w_c and the asymptotic growth parameter α of the number of skeleton paths:

$$w_c = \begin{cases} w_{\rm RPA} & , \quad \alpha \leq \sqrt{Z-1}, \\ \left(\alpha + \frac{Z-1}{\alpha}\right) t & , \quad \alpha \geq \sqrt{Z-1}\,. \end{cases} \tag{23}$$

The band-edge energy given by (23) grows monotonically with increasing α until it reaches $w_{\rm FP}$ for $\alpha = Z-1$. The total number of nonretraceable skeleton paths of length l for the hole, irrespective of whether the spin background is restored or not, is $Z(Z-1)^{l-1}$. Thus $\alpha = Z-1$ would mean that the number of Néel background-restoring skeleton paths has the same growth behavior as the total number of skeleton paths. This is extremely implausible at dimensions $D \geq 3$. In this case the majority of nonretraceable closed random paths is largely free of points visited more than once, which means that to restore a Néel background the hole essentially has to walk twice through such a path. This implies that α should be close to $\sqrt{Z-1}$, rather than to $Z-1$. The above argument gets better the higher the dimensionality.

We conclude from the above consideration that we should expect the band edge to be close to $w_{\rm RPA}$, that, i.e., far away from $w_{\rm FP}$, for lattices at high dimension. At the same time, we wish to emphasize that we have not been able to make the above argument exact by a strict estimate of an upper bound smaller than $Z-1$ for the parameter α. We will see, however, in the next section that, even for the low-dimensional systems we have considered, our numerical data provide good evidence for the conjecture that $\alpha < Z-1$ is generally true.

To calculate exactly the propagator given by Eq. (21), one would need to determine the number of distinct background-restoring bare skeleton paths of all lengths, which is a very complicated problem. In the next section we describe how we have overcome this problem for the concrete cases of a double chain and a square lattice Néel backgrounds.

III. RESULTS AND DISCUSSION

As mentioned in the previous section, we did find a way to estimate the numbers of different bare skeleton paths for all lengths and thus, through Eq. (21), obtain the propagator of a hole on a Néel background in two special cases. In this section, we will first describe our estimation in general, and in the two following subsections present and discuss the results we obtained for the density of states and spectral density, in the cases of a double chain and a square lattice.

To be specific, we first determined numerically the exact numbers of different Néel background-restoring skeleton paths for as many path lengths as our computer facilities allowed. For the case of a double chain we obtained all skeleton paths up to a length of 32 steps, and for lengths 34 and 36 we only determined the closed paths. The results are presented in Table I. For the square lattice Néel background we obtained all skeleton paths up to length 24. In Table II we exhibit these numbers.

From the numbers of skeleton paths exactly obtained, we determined the asymptotic behavior as a function of path length exhibited by our data. This we could adequately fit by the following functional form depending on three parameters:

$$K^l_{i,j} \simeq \frac{C_{i,j}\,\alpha^l}{l^{\beta_{i,j}}}, \qquad \forall\, i,j. \tag{24}$$

Notice the exponential dependence with the length which leads to the band-edge value given by Eq. (23), as described in the previous section. We determined the parameter α from fitting the data for the local propagator, the numbers of closed skeleton paths. The band edge of the energy spectrum which we determine from the local propagator is a "global" quantity, in the sense that it has to contain all poles of the Green's function, and the nonlocal Green's functions should not extend beyond this edge. Taking the latter fact into account and also to avoid spurious singularities in the self-energy obtained, we took the parameter α from the local propagator fit and fixed it while fitting the nonlocal propagators. The denominator in Eq. (24), depending on the parameter β, will essentially account for the energy dependence of the propagator near the band edge. Finally we included a proportionality constant, the parameter C.

In Tables III and IV we detail the asymptotes obtained for the double chain and the square lattice respectively. The asymptotes were obtained by a weighted fit to Eq. (24) of our exact short range data, attaching to the latter a dispersion decreasing with path length.

TABLE I. Exact numbers of nonretraceable Néel background-restoring skeleton paths on a double chain, classified according to path length or number of steps (l), and distance (d) between origin and end point, measured in units of the lattice parameter. Due to symmetry in the double chain, $n^s_{d^2} = 2$ different sites are end points with the same $d(\neq 0)$, thereby contributing equally to $n^l_{(d^2)}$.

l	$n^l_{(d^2=0)}$	$n^l_{(d^2=2)}$	$n^l_{(d^2=4)}$	$n^l_{(d^2=10)}$	$n^l_{(d^2=16)}$	$n^l_{(d^2=26)}$	$n^l_{(d^2=36)}$	$n^l_{(d^2=50)}$	n^l_{tot}
6	0	4	0	0	0	0	0	0	4
10	0	4	8	0	0	0	0	0	12
12	4	4	6	0	0	0	0	0	14
14	18	8	12	20	0	0	0	0	58
16	36	56	30	28	0	0	0	0	150
18	120	132	66	56	42	0	0	0	416
20	270	488	302	192	100	0	0	0	1352
22	846	1336	808	364	254	96	0	0	3704
24	2400	3736	2610	1468	880	300	0	0	11394
26	7052	11180	7812	4476	2236	880	214	0	33850
28	21432	32500	23006	14756	7584	3376	844	0	103498
30	63538	99900	71162	45688	23898	10100	2836	476	317598
32	193448	304628	217352	141920	78162	35228	11428	2280	984446
34	590154	-	-	-	-	-	-	-	-
36	1824844	-	-	-	-	-	-	-	-

We employed a general linear least squares fit solved by a singular value decomposition.[16] In particular, for the numbers of different skeleton paths of l steps extending from the origin i to the end point j defined by the propagator considered, which were obtained numerically, we considered a standard deviation σ_l:

$$\sigma_l \propto e^{-0.3l}. \tag{25}$$

Considering all data equally weighted one arrives at asymptotes similar to those presented here, but taking a path-length-dependent weight attached to the exact short range data will certainly produce a better representation of the asymptotic behavior for long path lengths. To quantify this, we can mention that the relative deviation of the number of skeleton paths from the asymptotes tabulated is of the order of 10^{-4} (double chain) and 10^{-3} (square lattice) for the longest paths exactly investigated. With the weighted fit (25) which we employed we could minimize spurious effects in our results, such as negative peaks in the spectral density. It is important to remark that the α parameter we obtain, which determines the band edge, is very stable to the consideration of different fits. We checked this by comparing weighted fits (25) with other exponents of e^{-l}, including the equal-weight case, and considering other functional forms for the standard deviations of the data. In all cases the α parameter obtained was well within 2% of the value presented in this work for the double chain, and 8% for the square lattice where fewer exact data from which to obtain the asymptote are available.

Having obtained the asymptotes for the skeleton-path numbers, and taking into account that for short path lengths (say, up to length l_0) we know the exact values of these (K) numbers, we evaluated the propagator given by Eq. (21) in the following way:

TABLE II. Exact numbers of nonretraceable Néel background-restoring skeleton paths on a square lattice, classified according to path length or number of steps (l), and distance (d) between origin and end point, measured in units of the lattice parameter. Due to symmetry, $n^s_{d^2}$ different sites are end points with the same d (see row in brackets).

l ($n^s_{d^2}$)	$n^l_{(d^2=0)}$ (1)	$n^l_{(d^2=2)}$ (4)	$n^l_{(d^2=4)}$ (4)	$n^l_{(d^2=8)}$ (4)	$n^l_{(d^2=10)}$ (8)	$n^l_{(d^2=16)}$ (4)	$n^l_{(d^2=18)}$ (4)	$n^l_{(d^2=20)}$ (8)	$n^l_{(d^2=26)}$ (8)	$n^l_{(d^2=32)}$ (4)	n^l_{tot}
6	0	8	0	0	0	0	0	0	0	0	8
10	0	16	32	0	0	0	0	0	0	0	48
12	8	16	24	32	0	0	0	0	0	0	80
14	72	192	120	32	80	0	0	0	0	0	496
16	440	528	384	208	368	0	0	0	0	0	1928
18	1728	2912	1488	768	1056	168	0	128	0	0	8248
20	8512	12176	7408	4072	5296	656	256	640	0	0	39016
22	33224	58648	35400	15072	19904	3224	2312	2832	384	0	171000
24	151224	257472	159376	76712	102528	16208	10608	13600	3824	512	792064

TABLE III. Double chain: Asymptotes obtained for $K^l_{i,j}$ [as defined by Eq. (24)]. In the first column we enter the relative position of end point j with respect to the origin i, denoting by $n(i)$ an nth nearest neighbor site of the origin i. For clarity, in the second column we write the distance d between i and j (squared). The last column indicates which $(n^l_{d^2}/n^s_{d^2})$ data (from Table I) were employed to determine each asymptote by the weighted fit [Eq. (25)], by stating the respective l.

j	d^2	α	$\beta_{i,j}$	$C_{i,j}$	l
$j=i$	0	1.88136	2.39084	1.26191	22-36
$2(i)$	2	1.88136	2.27482	0.66616	22-32
$3(i)$	4	1.88136	2.17748	0.33958	22-32
$6(i)$	10	1.88136	1.76242	5.278×10^{-2}	22-32
$7(i)$	16	1.88136	1.42770	9.05×10^{-3}	22-32
$10(i)$	26	1.88136	0.86016	5.7×10^{-4}	22-32

$$G^N_{i,j}(w) = G_{\rm RPA}(w)\delta_{i,j} + \sum_{l\geq 2}^{\infty}\left(\frac{C_{i,j}\alpha^l}{l^{\beta_{i,j}}}\right)G_l(w) + \sum_{l\geq 2}^{l_0}\left(K^l_{i,j} - \frac{C_{i,j}\alpha^l}{l^{\beta_{i,j}}}\right)G_l(w). \quad (26)$$

The second term in the above expression represents our estimation of the asymptotic or long skeleton-path contributions extrapolated to all path lengths, while the last term is a correction to include exactly the short range contributions evaluated numerically. It is an important detail that the infinite series appearing in Eq. (26) is related to the polylogarithm function

$$f_\beta(z) = \sum_{n=1}^{\infty}\frac{z^n}{n^\beta}, \quad (27)$$

for which the analytic continuation beyond the radius of convergence ($|z| = 1$) is well known. We obtained the numerical values for this function employing the MATHEMATICA program.[17]

Having evaluated the local propagator as described by Eq. (26) we determined the density of states $\rho(w)$,

$$\rho(w) = -\frac{1}{\pi}{\rm Im}[G_{i,i}(w)], \quad (28)$$

and the Fourier transform of the propagator in real space as

$$G(\mathbf{k},w) = \sum_{\mathbf{R}_j} e^{-i\mathbf{k}\cdot\mathbf{R}_j}G_{0,j}(w). \quad (29)$$

We define the spectral density as

$$A(\mathbf{k},w) = -\frac{1}{\pi}{\rm Im}[G(\mathbf{k},w)] \quad (30)$$

and the self-energy $\Sigma(\mathbf{k},w)$ by

$$G(\mathbf{k},w) = \frac{1}{w-\Sigma(\mathbf{k},w)}. \quad (31)$$

In the following we will present the results we obtained for these quantities, and discuss the similarities with the results which Zhong *et al.*[14] obtained employing the Lanczos spectra decoding method.

A. Double chain

In Fig. 1 we plot the density of states obtained for the double chain with the method described above, and, to compare, include the RPA density of states in the figure. We obtain a shift of the band edge, $w_c = 2.94t$, from the RPA value ($w_{\rm RPA} = 2.83t$) towards the Nagaoka energy ($w_{\rm FP} = 3t$), in accordance with the α parameter obtained (see Table III): $\alpha_{\rm RPA} = \sqrt{2} < \alpha \simeq 1.88 < \alpha_{\rm FP} = 2$. This result was referred to already in Sec. II. The good estimation we obtain for α (independent of

TABLE IV. Square lattice: Asymptotes obtained for $K^l_{i,j}$ [as defined by Eq. (24)]. In the first column we enter the relative position of end point j with respect to the origin i, denoting by $n(i)$ an nth nearest neighbor site of the origin i. For clarity, in the second column we write the distance d between i and j (squared). The last column indicates which $(n^l_{d^2}/n^s_{d^2})$ data (from Table II) were employed to determine each asymptote by the weighted fit [Eq. (25)], by stating the respective l.

j	d^2	α	$\beta_{i,j}$	$C_{i,j}$	l
$j=i$	0	2.31204	2.18809	0.29007	16-24
$2(i)$	2	2.31204	1.76948	3.298×10^{-2}	16-24
$3(i)$	4	2.31204	1.56262	1.056×10^{-2}	16-24
$5(i)$	8	2.31204	1.67271	7.07×10^{-3}	16-24
$7(i)$	10	2.31204	1.74651	5.95×10^{-3}	16-24
$9(i)$	16	2.31204	1.05138	2.1×10^{-4}	18-24
$11(i)$	18	2.31204	1.75567	1.29×10^{-3}	22-24
$12(i)$	20	2.31204	1.40003	2.7×10^{-4}	18-24

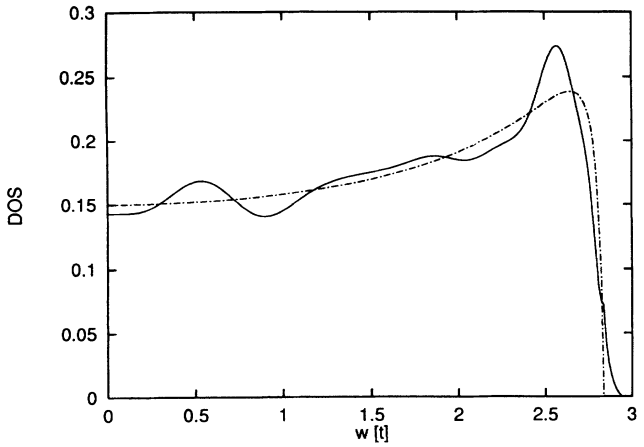

FIG. 1. Double chain. Density of states: our result (solid line); retraceable-path approximation, RPA (dot-dashed line).

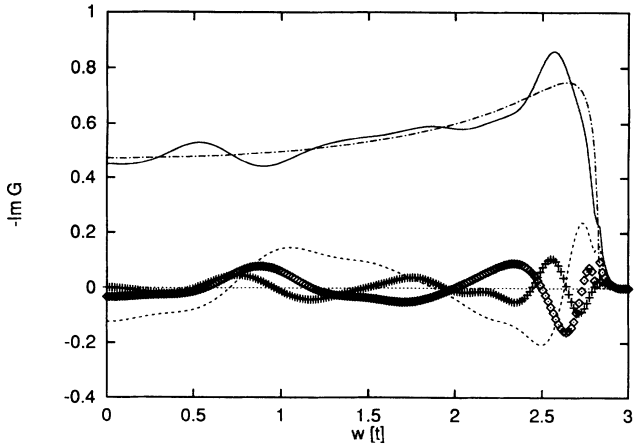

FIG. 2. Double chain. Imaginary part of the local propagator (solid line), of the RPA (local) propagator (dot-dashed line); of the nonlocal propagator between the origin and second (dashed line), third (boxes), and sixth nearest neighbors (crosses).

the asymptotic fit within 2%), and thereby for the band edge, indicates the absence of band tails extending to the Nagaoka energy for the double chain. The parameter β determines the shape of the density of states near the band edges via $\rho(w) \propto (w_c^2 - w^2)^{\beta-1}$.

We obtain a density of states remarkably similar to Zhong *et al.*,[14] not only in the main features present but quantitatively as well. In particular, there is a broad peaklike structure near the band edge, which we identified as due to the asymptotic behavior, second term in Eq. (26), corresponding to long skeleton-path contributions to $G_{i,i}$. In fact, short range contributions, which are exactly accounted for by the third term in Eq. (26), are producing a partial cancellation of the peak which would be obtained due to long skeleton-path contributions. In the density of states we can also identify a broad shoulder at intermediate energies and a second shoulder at lower energies as arising due to the short skeleton-path contributions, which we exactly calculate here.

To compare the orders of magnitude of the different contributions involved in $G(\mathbf{k}, w)$ of Eq. (29), we depict in Fig. 2 the imaginary part of the local propagator and the most relevant nonlocal Green's functions between nearest neighbors. We recognize a quick decrease in relative weight as one considers neighbors farther apart. This means that we obtain good convergence for the Fourier transform of the Green's function, $G(\mathbf{k}, w)$, by including the contributions up to tenth nearest neighbors.

In Fig. 3 we plot the spectral density (30) as a function of energy, for three different values of momentum $\mathbf{k}$. The spectral weight distribution is in general agreement with the results of Zhong *et al.*[14] Concretely, for $\mathbf{k} = (0, 0)$ we obtain a peaklike structure near the band edge and a broad shoulder at lower energies, both features present in Ref. 14 with slight differences in magnitude. We investigated the origin of those features, and found that the band-edge peak is determined by the asymptotic or longer skeleton-path contributions to the $\mathbf{k}$-dependent Green's function (where the local and the nonlocal propagator to second nearest neighbors are the dominant terms). The short range contributions tend to narrow and decrease the weight of the peak. It is interesting to note that the nonlocal propagators contributing to $G(\mathbf{k}, w)$ tend to shift the peak arising from the local propagator towards the band edges and to increase its weight. Meanwhile, the broad shoulder at intermediate energies originates from the short range contributions to the nonlocal propagators (mainly those corresponding to second and third nearest neighbors). In our case the main peak appears accompanied by a narrow secondary peak which is a totally spurious trace of the RPA band edge, mainly appearing in the nonlocal propagators, of no relevance whatsoever.

To exhibit the dispersion, in Fig. 3 we also plot the spectral density for $\mathbf{k} = (\frac{3\pi}{4}, 0)$ and $\mathbf{k} = (\pi, 0)$. Again here we observe the same weight distribution exhibited by the data of Zhong *et al.*,[14] where $A(\mathbf{k} = (\frac{3\pi}{4}, 0), w)$ contains the highest peaklike structure near the band edge in

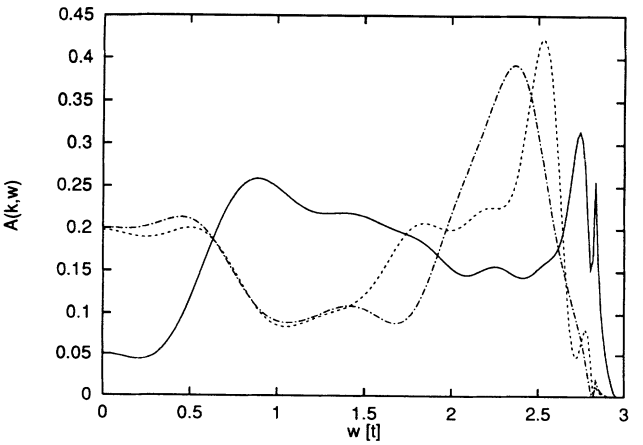

FIG. 3. Double chain. Spectral density $A(\mathbf{k}, w)$ as a function of energy for $\mathbf{k} = (0, 0)$ (solid line), $\mathbf{k} = (\frac{3\pi}{4}, 0)$ (dashed line), $\mathbf{k} = (\pi, 0)$ (dot-dashed line).

the whole Brillouin zone, while this structure is broadest for the $\mathbf{k} = (\pi, 0)$ data. Also the peak shifts towards the center of the band agree with those obtained in Ref. 14. For the $\mathbf{k} \neq 0$ cases, we find that the short range part of the nonlocal propagators contributing to $G(\mathbf{k}, w)$ are increasing the weight of the peak which would arise from the local propagator and shifting it towards the center of the band. The same short range part of the nonlocal propagators is responsible for the decrease in spectral weight obtained at intermediate energies [where for $\mathbf{k} = (0, 0)$ the broad shoulder appeared] and for the increase of weight in the center of the band.

Finally, in Fig. 4 we plot the self-energy obtained for the same $\mathbf{k}$ values taken for the spectral density results, and, for purposes of comparison, we include the dispersionless RPA self-energy. The effects of dispersion are clearly observable, and important departures from RPA are obtained. In Fig. 4(a) we plot the real part of the self-energy. The $\mathbf{k} = (0, 0)$ data show maximum departures from RPA for energies near the center of the band, while for the other $\mathbf{k}$ values these appear shifted towards intermediate energies. The origin of these departures lies mainly in the short range parts of the nonlocal propagators. Similar comments apply to the imaginary part of the self-energy plotted in Fig. 4(b). For $\mathbf{k} = (0, 0)$, we obtain an important reduction of the lifetime as compared to the RPA for energies near the center of the band.

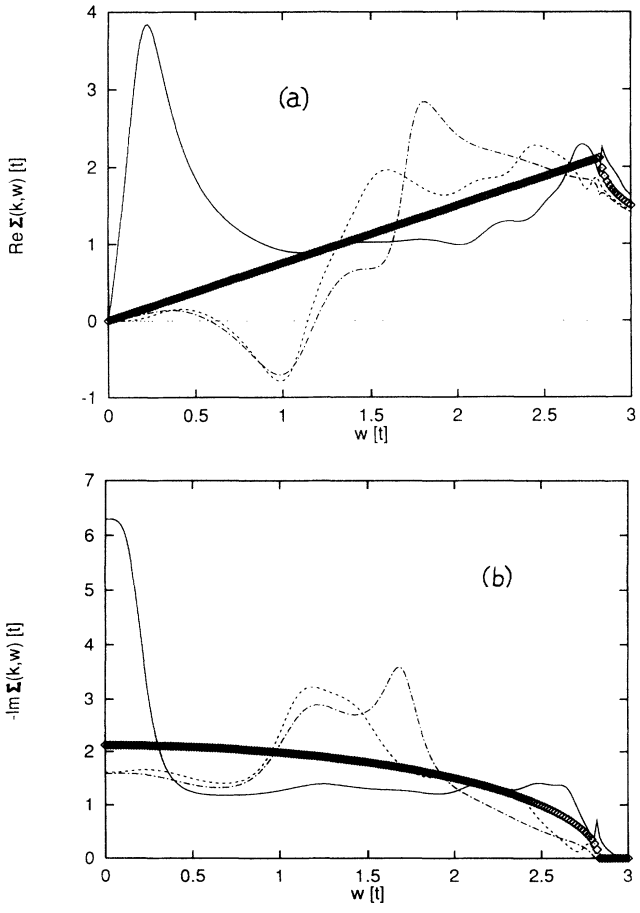

FIG. 4. Double chain. Self-energy $\Sigma(\mathbf{k}, w)$ of the hole as a function of energy: (a) Real part. (b) Imaginary part. RPA (boxes); $\mathbf{k} = (0, 0)$ (solid line), $\mathbf{k} = (\frac{3\pi}{4}, 0)$ (dashed line), $\mathbf{k} = (\pi, 0)$ (dot-dashed line).

B. Square lattice

In Fig. 5 we plot the density of states we obtained for the square lattice. As for the double chain, we obtain a shift of the band edge, $w_c = 3.61t$, from the RPA value ($w_{\mathrm{RPA}} = 3.46t$) towards the Nagaoka energy ($w_{\mathrm{FP}} = 4t$). This is determined by the α parameter obtained from the asymptotic fit (see Table IV) through Eq. (23): $\alpha_{\mathrm{RPA}} = \sqrt{3} < \alpha \simeq 2.31 < \alpha_{\mathrm{FP}} = 4$. As commented before, the reliability of our estimation for α (within 8%) clearly indicates the absence of band tails extending to the Nagaoka energy in the spectrum of the square lattice. This result also confirms our conjecture of Sec. II that the band-edge departures from the Nagaoka energy increase with dimensionality.

The almost featureless density of states, with minor departures from the RPA result as expected from the estimations in terms of the dimension mentioned in the Introduction, agrees with that obtained by Zhong *et al.*[14] apart from some minor oscillations. These oscillations result from the short skeleton-path contributions to the local propagator. In contrast to the double chain, here the only observable departure from the RPA density of states resulting from the asymptotic behavior is the band-edge shift.

In Fig. 6 we depict the imaginary part of the local propagator, and the most relevant nonlocal Green's functions between nearest neighbors. Again, a quick decrease in weight appears on considering neighbors farther apart, but this plot shows that nonlocal propagators have much less weight than the local one in comparison to the double chain (see also Fig. 2). This agrees with the estimation of the importance of nonlocal corrections to the RPA propagator as a function of the dimension mentioned in our Introduction. For the square lattice we obtained the

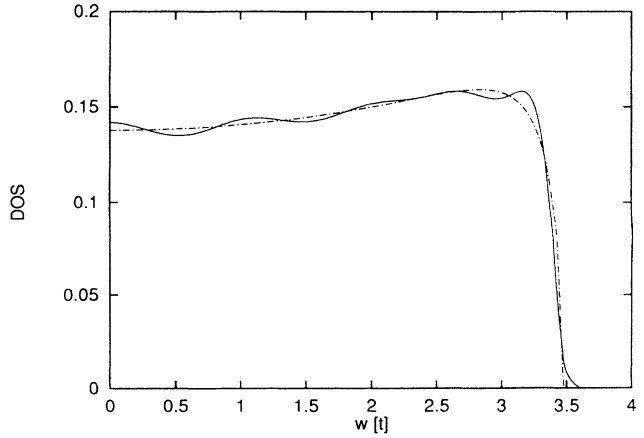

FIG. 5. Square lattice. Density of states: our result (solid line); retraceable-path approximation, RPA (dot-dashed line).

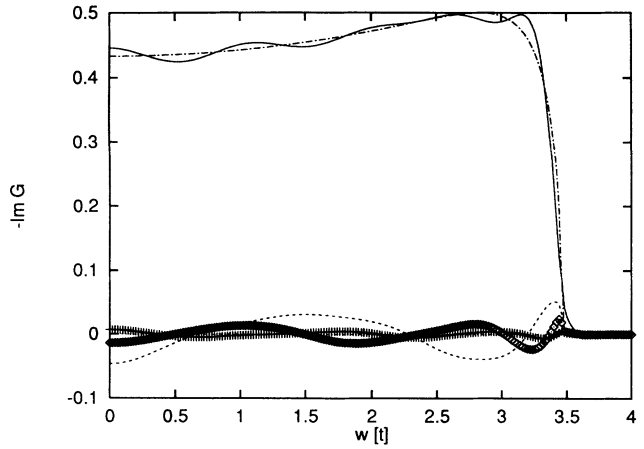

FIG. 6. Square lattice. Imaginary part of the local propagator (solid line), of the RPA (local) propagator (dot-dashed line); of the nonlocal propagator between the origin and second (dashed line), third (boxes), and fifth nearest neighbors (crosses).

spectral density including in the Fourier transform of the Green's function, $G(\mathbf{k}, w)$, contributions up to those of 12th nearest neighbors.

In Fig. 7 we plot the spectral density as a function of energy, for three different values of momentum $\mathbf{k}$. Here for $\mathbf{k} = (0,0)$ we obtain a low peaklike structure near the band edge and a shoulder at lower energies, which is broader than the one in Ref. 14 where the data seem to have been insufficient to enable them to trace the complete spectral density curve. Both structures result mainly from the short range part of the nonlocal propagators contributing to $G(\mathbf{k}, w)$. The effect of dispersion on the spectral weight distribution is coincident with that shown by Zhong *et al.*[14] In Fig. 7 we also plot the spectral density for $\mathbf{k} = (\pi, 0)$, which exhibits the highest and broadest peaklike structure, and $\mathbf{k} = (\frac{\pi}{2}, \frac{\pi}{2})$, which shows three maxima, all in accordance with Ref. 14. Again, the short range part of the nonlocal propagators contributing

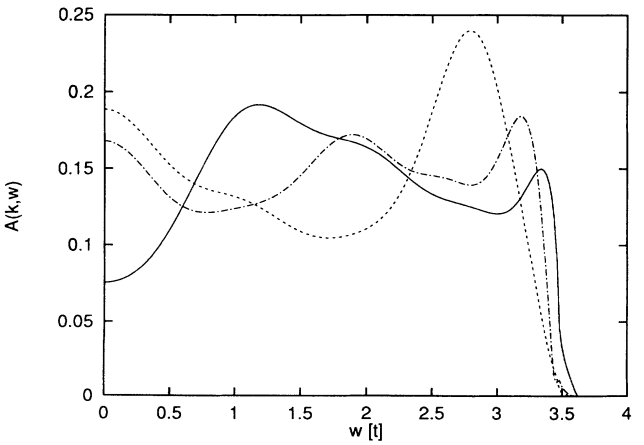

FIG. 7. Square lattice. Spectral density $A(\mathbf{k}, w)$ as a function of energy for $\mathbf{k} = (0,0)$ (solid line), $\mathbf{k} = (\pi, 0)$ (dashed line), $\mathbf{k} = (\frac{\pi}{2}, \frac{\pi}{2})$ (dot-dashed line).

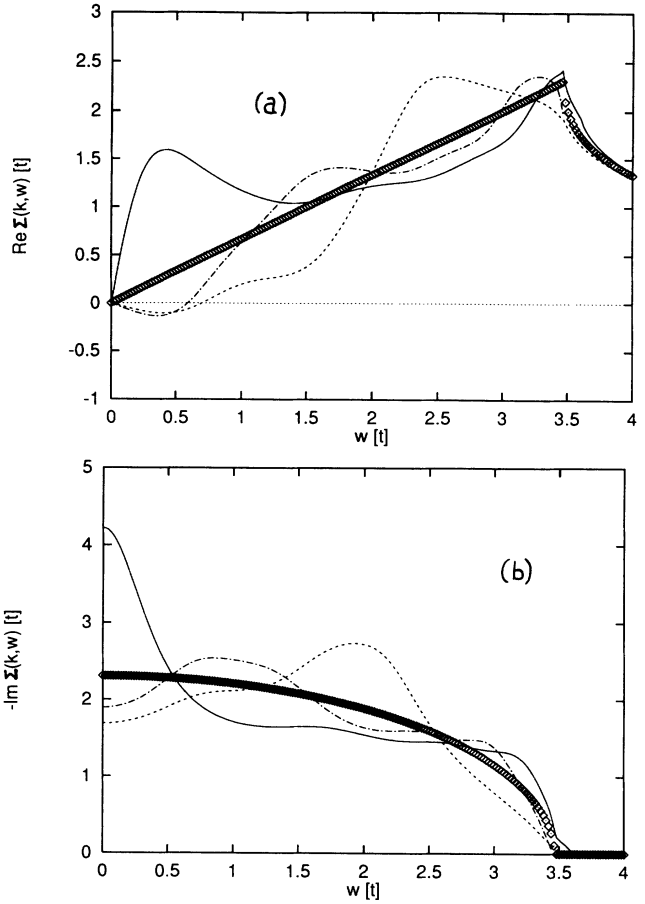

FIG. 8. Square lattice. Self-energy $\Sigma(\mathbf{k}, w)$ of the hole as a function of energy: (a) Real part. (b) Imaginary part. RPA (boxes); $\mathbf{k} = (0,0)$ (solid line), $\mathbf{k} = (\pi, 0)$ (dashed line), $\mathbf{k} = (\frac{\pi}{2}, \frac{\pi}{2})$ (dot-dashed line).

to $G(\mathbf{k}, w)$ accounts for this distribution of weight.

In Fig. 8 we plot the self-energy obtained for the same $\mathbf{k}$ values taken for the spectral density, including the dispersionless RPA self-energy for hole motion on a square lattice with Néel spin order. The qualitative effects of dispersion are similar to those obtained for the double chain, but the departures from RPA obtained are smaller, as expected. As before, the departures obtained mainly result from the short range part of the nonlocal propagators.

IV. SUMMARY

In this work we studied the motion of a hole on a Néel background, neglecting spin fluctuations, in the framework of the Nagaoka expansion for the Green's function. Starting from the retraceable-path approximation, known to become exact in the one- and infinite-dimensional cases, where no dispersion appears, we derived a resummation of the Nagaoka expansion by considering nonretraceable skeleton paths and dressing them by retraceable-path insertions. The contribution of each of such dressed skeleton paths was evaluated exactly. The problem is then reduced to the determination of the numbers of different bare skeleton paths of each length. We

numerically exactly obtained these numbers up to length 36 for the double chain, and 24 for the square lattice. From these numbers, we determined an asymptotic extrapolation for all path lengths, and used all this information to evaluate the Green's function. We then determined the density of states and spectral density for the double chain and square lattice cases. We determine the band edges through a growth parameter α obtained in the asymptotic fit. The reliability of our determination of this parameter, placing the band edge at a value between the RPA edge and the Nagaoka energy, points towards the absence of band tails extending to the Nagaoka energy in the spectrums of the double chain and the square lattice. At the same time, this confirms our conjecture about the increase of the band-edge departures from the Nagaoka energy with dimensionality. Our results deviate from the exact solution of the problem only due to the differences between our asymptotic extrapolation and the unknown exact numbers of skeleton paths longer than 36 steps for the double chain and 24 for the square lattice. That these deviations are small is confirmed by the general coincidence of our density of states and spectral density results with those obtained through the Lanczos approach by Zhong *et al.*[14] Our "analytic" approach has the added advantage of determining the relevant hole paths responsible for the main features present in the density of states and the spectral density.

ACKNOWLEDGMENTS

This research was performed within the scientific program of the Sonderforschungsbereich 341, supported by the Deutsche Forschungsgemeinschaft. We would like to acknowledge useful discussions and comparison with Lanczos results by C. A. Balseiro and K. A. Hallberg. We thank S. Sorella for sending us his results prior to publication, and P. Horsch, D. Vollhardt, and J. M. J. van Leeuwen for discussions on their related work.

*Future address: Dept. of Theoretical Physics, Univ. of Oxford, 1 Keble Road, Oxford OX1 3NP, United Kingdom.

[1]L. N. Bulaevskii, E. L. Nagaev, and D. I. Khomskii, Sov. Phys. JETP **27**, 836 (1968).

[2]W. F. Brinkman and T. M. Rice, Phys. Rev. B **2**, 1324 (1970).

[3]Y. Nagaoka, Solid State Commun. **3**, 409 (1965); Phys. Rev. **147**, 392 (1966).

[4]W. Metzner, P. Schmit, and D. Vollhardt, Phys. Rev. B **45**, 2237 (1992).

[5]R. Strack and D. Vollhardt, Phys. Rev. B **46**, 13852 (1992).

[6]S. A. Trugman, Phys. Rev. B **37**, 1597 (1988).

[7]B. I. Shraiman and E. D. Siggia, Phys. Rev. Lett. **60**, 740 (1988).

[8]S. Schmitt-Rink, C. M. Varma, and A. E. Ruckenstein, Phys. Rev. Lett. **60**, 2793 (1988).

[9]C. L. Kane, P. A. Lee, and N. Read, Phys. Rev. B **39**, 6880 (1989).

[10]H. Tsunetsugu and Y. Takahashi, J. Phys. Soc. Jpn. **58**, 4184 (1989).

[11]J. Inoue and S. Maekawa, J. Phys. Soc. Jpn. **59**, 2110 (1990).

[12]K. J. v. Szczepanski, P. Horsch, W. Stephan, and M. Ziegler, Phys. Rev. B **41**, 2017 (1990); A. Ramšak and P. Horsch, *ibid.* **48**, 10559 (1993).

[13]E. Dagotto, R. Joynt, A. Moreo, S. Bacci, and E. Gagliano, Phys. Rev. B **41**, 9049 (1990).

[14]Q. F. Zhong, S. Sorella, and A. Parola, Phys. Rev. B **49**, 6408 (1994).

[15]C. A. Balseiro (private communication).

[16]W. H. Press, B. P. Flannery, S. A. Teukolsky, and W. T. Vetterling, *Numerical Recipes: The Art of Scientific Computing*, 2nd ed. (Cambridge University Press, Cambridge, England, 1992).

[17]S. Wolfram, *Mathematica: A System for Doing Mathematics by Computer*, 2nd ed. (Addison-Wesley, Redwood City, 1991), p. 575.